Use of Quantum Methods with Transition State Theory: Application to H-Atom Metathesis Reactions†

Juan P. Senosiain,‡ Charles B. Musgrave,§ and David M. Golden*,⊥

Department of Mechanical Engineering, Department of Materials Science and Engineering, and Department of Chemical Engineering, Stanford University, Stanford, California 94305

Received: July 6, 2000; In Final Form: November 7, 2000

The use of quantum chemical methods to determine rate constants for some H-atom metathesis reactions using transition state theory and tunneling corrections is explored. Comparisons are made among several methods (DFT, MP2, QCISD), all of which yield similar structures and frequencies for the transition states, but quite different barrier heights. Tunneling corrections are made using either the well-known Eckart method or one based on the WKB approach. We find that we can fit the extant data by varying the barrier heights using either tunneling approach, although the WKB method is both more accurate and more labor intensive. Values of the barrier heights obtained this way are not in good agreement with those obtained from any of the quantum methods.

Introduction

Understanding and modeling complex chemical systems requires the ability to construct a mechanism, and assign rate coefficients to the elementary steps that constitute the mechanism, followed by the solution of the coupled differential equations that ensue. Application to problems in the realm of atmospheric and combustion processes represents examples where much effort has been expended. A way to approach such models is to use the methods of constrained optimization illustrated in the mechanism development for the combustion of natural gas, known as GRI-Mech.[1] Such methods require a "reasonably" accurate first estimate of each rate coefficient, so that the optimization does not explore false pathways. Thus, there exists the need for a semiquantitative "screening tool". All too often, knowledge of reaction rate coefficients is needed at temperatures outside the range of preexisting experimental data. These rate coefficients may be different from the experimental values by several orders of magnitude. In this paper, we present a methodology using quantum chemistry, canonical transition state theory, and a WKB approach to tunneling corrections to extrapolate experimental data over a broad temperature range. We compare this method to the use of Eckart[2] corrections.

We apply this methodology for the series of hydrogen abstraction reactions:

$$C_2H_6 + X \rightarrow C_2H_5 + HX$$

where X = H, O, OH, NH_2, CH_3, as well as to C_2D_6 for X = OH. We have chosen this set of reactions because they are of interest to both combustion and atmospheric chemists, and experimental data can be available in the 250−2000 K range. Our goal is to use quantum chemical methods to compute the structure and frequencies and to extract the "true" (i.e., temperature independent) barrier from experimental data, so that we may compare quantum calculations of this quantity, with the longer term goal of being able to rely heavily on quantum methods for rate calculations.

Hydrogen abstraction from alkanes has been the subject of several ab initio studies.[3−7] In particular, the group at the National Institute of Standards and Technology (NIST)[8] has attempted to systematically correct, using the Eckart potential, the imaginary frequencies arising from quantum calculations. These are not expected to be reliable when the harmonic approximation breaks down. We have applied their method herein along with one of our own, based on WKB method. Other workers[5,9] have often allowed the imaginary frequency and thus the tunneling correction to be a fit parameter. This latter method will allow good representation of the reaction being considered, but does not lead to the hoped-for generalization that might be applied to other reactions.

Background

Benson has presented a facile method for evaluating thermochemical data and kinetic parameters of gas-phase reactions.[10] This method, usually called "thermochemical kinetics", is based on the use of canonical transition state theory. The effectiveness of this procedure in fitting experimental reaction rates[11,12] is remarkable considering that the frequencies of the transition state were estimated empirically, usually by taking partial bonds in transition states as half bonds and reducing the force constants associated with these bonds by a factor of 2, which reduces the frequencies to ∼70% of their values for a normal bond, and tunneling is not addressed. The success of these methods has been discussed by Rodgers.[13]

Calculational Procedure

Electronic Structure Calculations. In this work, quantum chemical calculations are employed primarily to ascertain the structure and frequencies of the transition state, reactants, and products. It is commonly assumed that ab initio methods result in larger errors for computed energies compared to those of predicted structures and frequencies. Although this is generally

† Part of the special issue "Harold Johnston Festschrift". The authors would like to express their gratitude to Harold Johnston for his invaluable contributions to our science and his continued inspiration.

* To whom correspondence should be addressed. E-mail: golden@sri.com. Fax: 650-723-1748.

‡ Department of Materials Science and Engineering.

§ Departments of Chemical Engineering and Materials Science and Engineering.

⊥ Department of Mechanical Engineering. Also associated with Molecular Physics Laboratory, SRI International, Menlo Park, CA 94025.

10.1021/jp002424l CCC: $20.00
Published on Web 01/03/2001

true, calculated frequencies can result in nonnegligible errors in the entropy and density of states, particularly in structures with internal rotors and loose frequencies. We used Becke's three-parameter method (B3LYP[14]) with the 6-311G(d,p) basis set for this purpose. It has been found elsewhere[15,16] that this method gives accurate geometries and frequencies, and furthermore, the basis-set dependence of these is only modest.

To obtain an assessment of the accuracy, geometry optimizations were also done using second-order Møller−Plesset perturbation theory[17] (MP2) and quadratic configuration interaction with singles and doubles excitations[18] (QCISD).[19] All electronic structure calculations were performed using the Gaussian collection of programs.[20] Standard formulas were used to evaluate the translational, vibrational, rotational, and electronic partition functions (see for example [21]).

Internal Rotations. Modes corresponding to internal rotations were removed from Q_{vib} and treated as hindered internal rotors, in the framework of the Pitzer and Gwinn approximation.[22] The reduced moments of inertia for internal rotations were corrected to first order for rotor−rotor coupling.[22] For X = OH, NH_2, and CH_3, we examined the internal rotation of that group in the transition state; in cases where the barriers to internal rotation were significant (i.e., >0.3 kcal/mol) and evidently asymmetric, the rotational potential was mapped by performing semirelaxed density functional theory (DFT) calculations and the partition function was evaluated using a Fourier representation of this potential with up to 4-fold components: (for the reactions treated herein, this only pertains to X = OH)

$$V(\phi) = V_0 + \frac{1}{2}\sum V_n[1 - \cos(n\phi)]$$

$$Q_{ir}^{hind} = \left(\frac{2\pi kT}{h^2}\right)^{1/2} \int_0^{2\pi/\sigma} I_r^{1/2} \exp[-V(\phi)/kT]\, d\phi$$

$$Q_{ir}^{PG} = \left(\frac{Q_{ho}^{q}}{Q_{ho}^{cl}}\right) Q_{ir}^{hind}$$

$$Q_{ho}^{q} = \frac{e^{-u/2}}{1 - e^{-u}}; \quad Q_{ho}^{cl} = \frac{1}{u}; \quad u = \frac{h\nu}{kT}$$

where σ is the symmetry number of the internal rotor, I_r is the reduced moment of inertia, and $Q_{ho}{}^{q}$ and $Q_{ho}{}^{cl}$ designate the quantum and classical harmonic oscillator partition functions.

Tunneling. Since all ab initio calculations we performed treated the atomic nuclei classically (in a Born−Oppenheimer fashion) an explicit correction is needed to account for tunneling. Since rigorous corrections for multidimensional tunneling are very computationally demanding, we computed 1-dimensional tunneling corrections along the reaction path where most of the nonclassical effects will occur. We calculated the transmission coefficient using two distinct methods.

Eckart Method. The first uses the asymmetric Eckart function to represent the potential along the reaction coordinate. The Schrödinger equation for this potential was solved analytically by Eckart:[23]

$$V(s) = \frac{A\zeta(s)}{(1 + \zeta(s))} + \frac{B\zeta(s)}{(1 + \zeta(s))^2}$$

$$\zeta(s) = \exp[2\pi s/L^*]$$

In this method we obtain these parameters from calculated forward and reverse energy barriers (ΔV_1 and ΔV_2) and the imaginary frequency (ν^*) corresponding to the reaction coordinate at the transition state:

$$A = (\Delta V_2 - \Delta V_1)$$

$$B = [\Delta V_2{}^{1/2} + \Delta V_2{}^{1/2}]^2$$

$$L^* = \frac{A^2 - B^2}{\sqrt{8}B^{3/2}\upsilon^*}$$

The imaginary frequencies output by electronic structure calculations may not be reliable if the potential energy surface is so flat that the harmonic approximation breaks down. In a variant of the Eckart method, to get a better representation of the potential energy surface near the transition state we performed a nonlinear fit of the Eckart function to a calculated potential along the intrinsic reaction coordinate (IRC[24,25]), adjusting all three parameters. The imaginary frequency is obtained directly from the curvature of the IRC potential at the transition state:

$$\upsilon^* = \frac{1}{2\pi c}\sqrt{-\left(\frac{\partial^2 V}{\partial s^2}\right)_{s\,max}}$$

WKB Method. The second method is based on the Wentzel−Kramers−Brillouin (WKB) solution for a particle tunneling through a square potential. [See any advanced quantum mechanics text, for example: Schiff, L. I. *Quantum Mechanics*; McGraw Hill Book Co.: New York, 1968.] If the IRC curve is a slowly varying function of the reaction coordinate, *s*, we can treat the potential as a juxtaposition of square barriers and the transmission coefficients will be multiplicative (provided that they are small, i.e., when most of the flux is reflected). The energy-dependent transmission probability over the entire barrier is given by the integral equation:

$$\kappa_{WKB}(E) = \exp\left[-\left(\frac{4\sqrt{2\pi}}{h}\right)\int_{a(E)}^{b(E)} \sqrt{(V(s) - E)}\, ds\right]$$

where $a(E)$ and $b(E)$ are the classical turning points at a given energy.

The overall tunneling correction is the ratio of the quantum-mechanical barrier-crossing rate to the classical-mechanical barrier-crossing rate:

$$\Gamma(T) = \frac{\exp(V_1/k_BT)}{k_BT}\int_0^\infty \kappa(E)\exp(-V_1/k_BT)\, dE$$

Fitting Protocol. To extract the energy barrier and rate constants using the WKB approach for tunneling, our protocol is as follows:

(a) Determine the tunneling coefficient $\Gamma(T)$ by integrating the IRC surface, then divide the experimental rate constants by this quantity.

(b) Using the moments of inertia and vibrational frequencies from the quantum chemical calculations, compute the partition functions of the transition state theory expression:

$$k_{TST} = \frac{k_BT}{h}\frac{Q'_{TS}}{Q_AQ_{BC}}\exp\left(\frac{-\Delta H_0^{\ddagger}}{k_BT}\right)$$

(c) Use the "corrected" experimental rate constants from (a) above and the calculated partition functions to find the best value of $\Delta H_0^{\ddagger}$ using canonical transition state theory. The temperature

TABLE 1: Principal Moments of Inertia (amu Å^2) and Frequencies (cm^{-1})

species	I_A	I_B	I_C	ν
TS(OH+C_2H_6)	20.17	102.16	114.19	454 **i**, (41),[a] 116, (178), 389, 769, 809, 875, 1013, 1130, 1224, 1250, 1352, 1410, 1442, 1479, 1488, 1498, 3016, 3054, 3077, 3094, 3123, 3743
TS(OH+C_2D_6)	130.77	115.85	29.47	386 **i**, (47), 106, (135), 295, 590, 601, 758, 832, 916, 977, 998, 1010, 1061, 1072, 1078, 1089, 1176, 2170, 2218, 2275, 2295, 2317, 3745
TS(H+C_2H_6)	10.66	27.93	32.14	1178 **i**, (196), 316, 573, 837, 878, 1019, 1116, 1198, 1213, 1238, 1409, 1468, 1492, 1493, 1681, 3004, 3059, 3078, 3088, 3155
TS(O+C_2H_6)	19.05	94.10	106.72	1363 **i**, 131, (153), 435, 552, 818, 825, 1009, 1086, 1195, 1235, 1242, 1408, 1467, 1479, 1493, 3002, 3065, 3074, 3099, 3145
TS(NH_2+C_2H_6)	19.69	107.22	117.90	1600 **i**, (18), 145, (169), 431, 480, 753, 771, 882, 935, 1039, 1195, 1228, 1338, 1405, 1466, 1485, 1494, 1494, 1565, 3002, 3057, 3068, 3089, 3131, 3379, 3469
TS(CH_3+C_2H_6)	22.24	108.92	121.42	1627 **i**, (32), 139, (165), 371, 476, 548, 678, 857, 909, 1032, 1143, 1176, 1226, 1388, 1389, 1409, 1449, 1450, 1466, 1495, 1496, 3002, 3051, 3053, 3062, 3078, 3130, 3182, 3183
C_2H_6	6.27	25.39	25.39	(307), 827, 827, 997, 1219, 1219, 1410, 1426, 1506, 1506, 1508, 1508, 3024, 3025, 3070, 3070, 3095, 3095
C_2H_5	4.87	22.25	24.00	(108), 476, 813, 980, 1061, 1192, 1401, 1466, 1483, 1483, 2941, 3033, 3076, 3136, 3235
H_2	0.28	0.28		4422
OH	0.90	0.90		3700
H_2O	0.63	1.16	1.79	1639, 3810, 3907
NH_2	0.74	1.30	2.04	1535, 3332, 3417
NH_3	1.71	1.71	2.67	1073, 1682, 1682, 3460, 3579, 3579

[a] Frequencies in parentheses were treated as internal rotors.

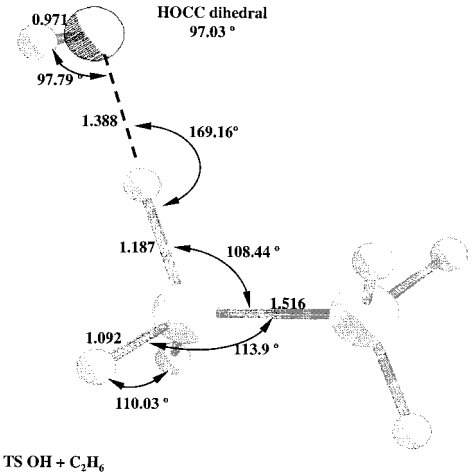

Figure 1. Transition state geometry for OH + C_2H_6 → C_2H_5 + H_2O reaction.

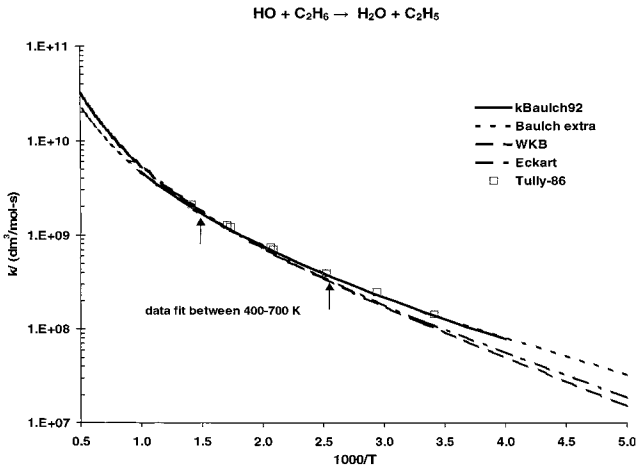

Figure 2. Arrhenius plot of rate constant and TST fits for OH + C_2H_6 → C_2H_5 + H_2O reaction. Arrows indicate the temperature range used for fitting TST rates. "92 Baulch extrapolated" indicates the range were there is no experimental data to support Baulch's 92 recommendation.

or temperature range used in this fitting procedure can be varied. Usually we used temperatures in the range of the experimental data where we expected less tunneling, but they were not so high that we expected larger uncertainty in the data itself.

(d) Multiply the rate constants by the $\Gamma(T)$.

(e) Generate three-parameter fits of the form

$$k(T) = AT^B \exp(-C/T)$$

If the asymmetric Eckart tunneling correction is used, an initial value for the activation barrier is needed. This can be obtained from experiments or ab initio calculations. Steps a−c above were repeated iteratively (except that $\Gamma(T)$ comes directly from the Eckart expression.) until self-consistency was obtained. This is followed by steps d and e.

Results and Discussion

Geometries and Vibrational Frequencies. The geometries of the transition states are fairly similar. The transition state for X = OH is shown in Figure 1. Principal moments of inertia and vibrational frequencies of reactants, products, and transition states are summarized in Table 1. Reduced moments of inertia of internal rotors and Fourier components of the rotational potential are shown in Table 2.

TABLE 2: Reduced Moments of Inertia (amu Å^2), Corresponding Frequencies (cm^{-1}) and Fourier Components of Internal Rotation Potential (cal/mol)

species	rotor	I_r	ν	V_0	V_1	V_2	V_3	V_4
C_2H_6	CH_3	1.56	307				3258	
C_2H_5	CH_3	1.09	108				467	
TS(H+C_2H_6)	CH_3	2.23	196				1935	
TS(O+C_2H_6)	CH_3	2.88	153				1517	
TS(OH+C_2H_6)	CH_3	3.02	178				2089	
TS(OH+C_2H_6)	OH	0.92	41	329	−195	−208	−42	−16
TS(OH+C_2D_6)	CD_3	5.54	135				2089	
TS(OH+C_2D_6)	OH	0.94	47	329	−195	−208	−42	−16
TS(NH_2+C_2H_6)	CH_3	2.98	168				2118	
TS(NH_2+C_2H_6)	NH_2	2.00	18				151	
TS($C'H_3$+C_2H_6)	CH_3	2.98	168				2118	
TS($C'H_3$+C_2H_6)	$C'H_3$	2.00	18				151	

OH + C_2H_6 → C_2H_5 + H_2O. Experimental data available for this reaction have been reported in the range 180−1000 K (see refs 7, 26, and 27 and references therein). There is some high temperature data (T > 1000) that scatters appreciably.[28] Reaction rates fit to the data in the 400−700 K range are shown in Figure 2. Our results agree well with the recommendation of Baulch et al.,[27] with the largest deviations (∼20%) occurring at the lowest temperatures. B3LYP predicts a very early

TABLE 3: Calculated, Fitted, and Experimental Activation Barriers $\Delta H_0^{\ddagger}$ (kcal/mol)

reaction	B3LYP[a]	MP2[b]	QCISD(T)[c]	TST fit (Eckart)	TST fit (WKB)	temp range (K)	Γ_{WKB} (300 K)
$H + C_2H_6 \rightarrow H_2 + C_2H_5$	4.94	15.96	11.04	9.69	9.72	400−700	3.60
$O + C_2H_6 \rightarrow OH + C_2H_5$	−0.59	8.45	3.44	6.35	6.34	400−700	3.71
$OH + C_2H_6 \rightarrow H_2O + C_2H_5$	−1.48	3.34	9.67	2.48	2.61	400−700	1.45
$OH + C_2D_6 \rightarrow HOD + C_2D_5$	−0.72	4.10	10.44	3.11	3.26	400−700	1.43
$NH_2 + C_2H_6 \rightarrow NH_3 + C_2H_5$	8.16	6.64		9.76	10.03	894−961	8.04
$CH_3 + C_2H_6 \rightarrow CH_4 + C_2H_5$	12.67	13.85	15.04	14.75	14.56	400−700	8.58

[a] B3LYP/6-311++G(3df,2p)//B3LYP/6-311G(d,p). [b] MP2/6-311++G(3df,2p)//B3LYP/6-311G(d,p). [c] QCISD(T)/6-311++G(3df,2p)//QCISD/6-311G(d,p).

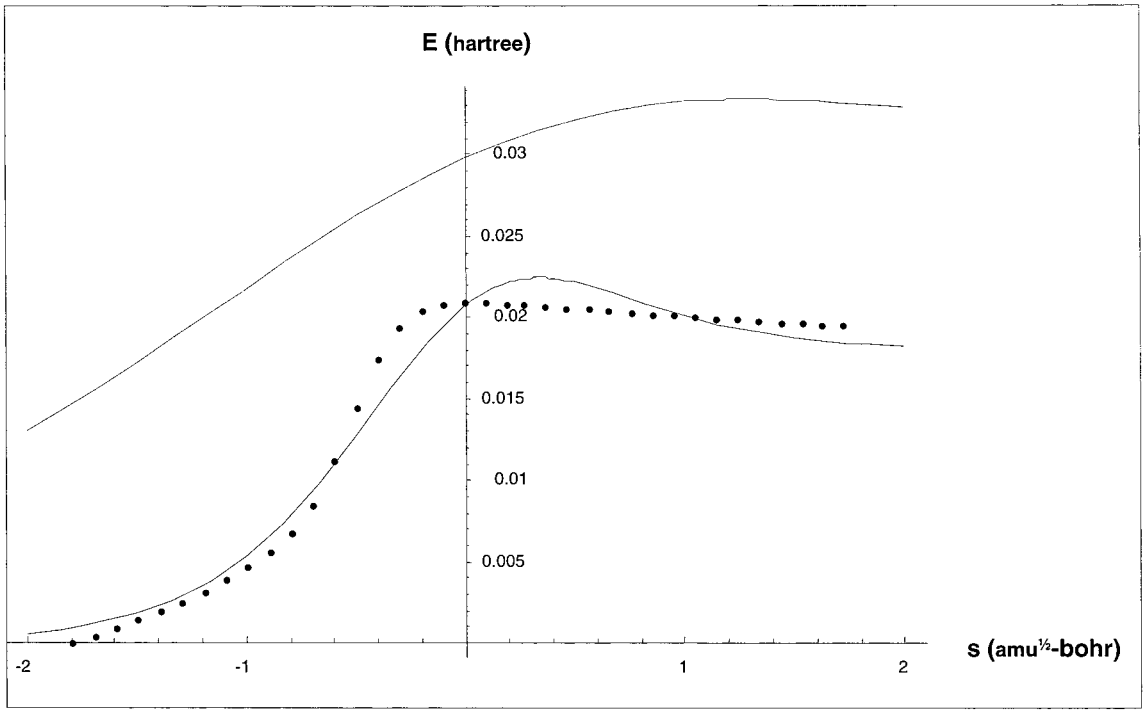

Figure 3. Three-parameter Eckart function for $OH + C_2H_6 \rightarrow C_2H_5 + H_2O$ reaction (energy vs mass-weighted distance). B3LYP IRC calculations are shown as dots, dashed line is the Eckart function with $\Delta H_0^{\ddagger} = 2.48$ (from a simple TST fit), $\Delta H_{298} = -18.48$ (the known heat of reaction), and $\nu^{**} = 454$ cm^{-1} (from the B3LYP calculation), solid line is the best fit to the IRC points with all three parameters allowed to vary yielding $\Delta H_0^{\ddagger} = 2.82$, $\Delta H = -11.27$ and $\nu^{**} = 930$ cm^{-1}.

transition state for this reaction, the HO−H and H−C_2H_5 bonds are elongated by 44.3 and 8.5% respectively, and the transition state (even corrected for zero-point energy) lies below the entrance channel in disagreement with experiment (see Table 3)! In contrast a QCISD, optimization yields a transition state where the transition state is not so early (HO−H and H−C_2H_5 bonds are strained by 35.2% and 11.3%) and 9.6 kcal/mol above the entrance channel, also in disagreement with experiment. A low barrier may suggest that a dynamic bottleneck of the reaction might not coincide with the transition state. This might explain the difference between our fitted energy barrier of 2.6 kcal/mol (WKB) and the 4.0 kcal/mol calculated by Truhlar and co-workers[29] using variational transition state theory.

For this reaction the shape of the energy surface along the reaction coordinate is poorly represented by a three-parameter Eckart function as seen in Figure 3. When Eckart tunneling calculations were performed using parameters derived by fitting the IRC calculation, as suggested by González,[24,25] the results are in close agreement with experiment even though the resulting Eckart potential has the wrong barrier and thermochemistry. The imaginary frequency of this forced Eckart potential increases from 454 to 930 cm^{-1} and the tunneling correction increases substantially (almost by 80% at 300 K). See Figure 4 for an Arrhenius representation of the tunneling.

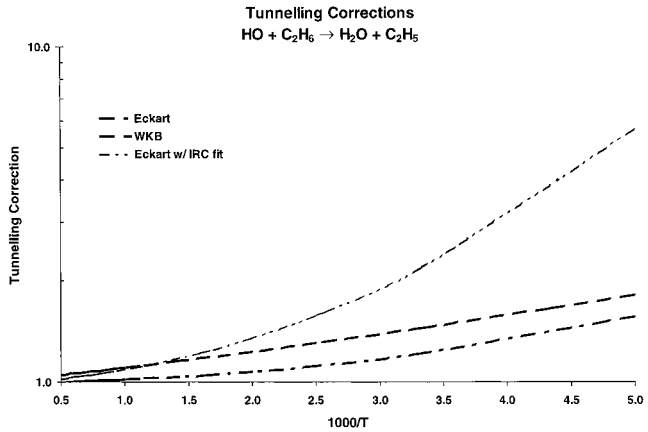

Figure 4. Eckart and WKB tunneling for the $OH + C_2H_6 \rightarrow C_2H_5 + H_2O$ reaction.

In this case as in all the others, we conclude that there is no real advantage to forcing the IRC derived potential to fit the somewhat arbitrary Eckart form. We suggest that the WKB approach be used if accuracy greater than the simple Eckart method is required.

Hindered Rotor. In order to accurately calculate the partition function of the OH hindered rotor we mapped a semirelaxed

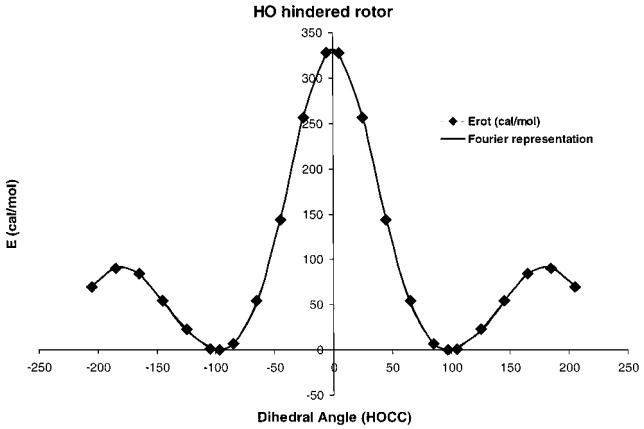

Figure 5. Rotational potential of OH rotor of the transition state for the OH + C_2H_6 → C_2H_5 + H_2O reaction. DFT calculations and approximating function

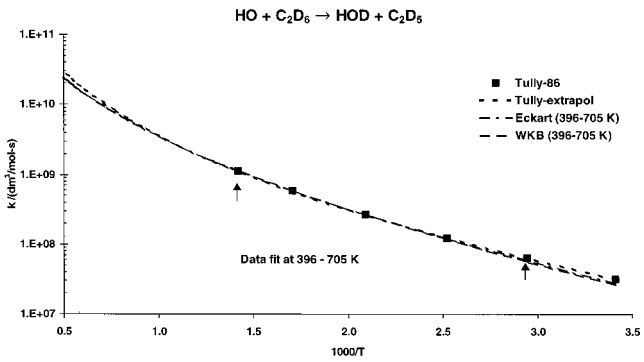

Figure 6. Arrhenius plot of rate constant and TST fits for OH + C_2D_6 → C_2D_5 + HOD reaction. Arrows indicate the temperature range used for fitting TST rates.

rotation potential (constraining only the O−C bond length) at the B3LYP/6-311G(d,p) level. A five-term Fourier function suffices to represent this potential, as can be seen in Figure 5. This can be readily used with the methods of Pitzer and Gwinn[22] to calculate the partition function and thermodynamic properties of the hindered rotor. (The difference between using this treatment and a simple pseudo 3-fold potential, as suggested by Benson,[10] may be marginal except where rotors are very asymmetrical and barriers are larger than 3−5 kcal/mol).

OH + C_2D_6 → C_2D_5 + HOD. This reaction has been measured in the range 293−705 K by Tully et al.[30] Both tunneling methods are in excellent agreement with these measurements (Figure 6). Although the calculated energies are identical regardless of the isotopes used, the IRC surfaces differ in shape because they are performed using mass-weighted coordinates. However, the barriers for OH + C_2H_6 and OH + C_2D_6 are sufficiently broad in both cases that the tunneling corrections for are almost identical. We conclude that most of the kinetic isotope effect (Figure 7) is due to the zero-point energy which lowers the activation barriers by different amounts.

H + C_2H_6 → C_2H_5 + H_2. We have chosen to fit data in the 400−700 K range and extrapolate our model to 300−2000 K, the range to which the Baulch et al. recommendation extends.[27] The results, shown in Figure 8, are not too different for the two methods of tunneling used. They agree well with the measurements of Purnell[31,32] and co-workers at mid-temperatures, as well as with Villermaux and Lede's[33] measurements down to 281 K. The largest deviations from the Baulch et al. recommendation occur at higher temperatures (T > 1000 K) where there is little experimental data. The fitted energy barriers are

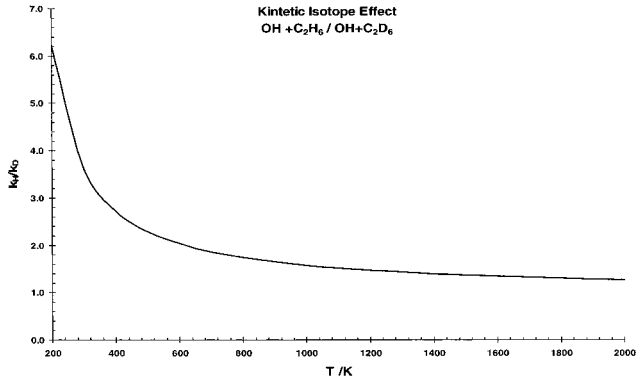

Figure 7. Kinetic isotope effect for OH + C_2H_6 → C_2H_5 + H_2O and OH + C_2D_6 → C_2D_5 + HOD reactions

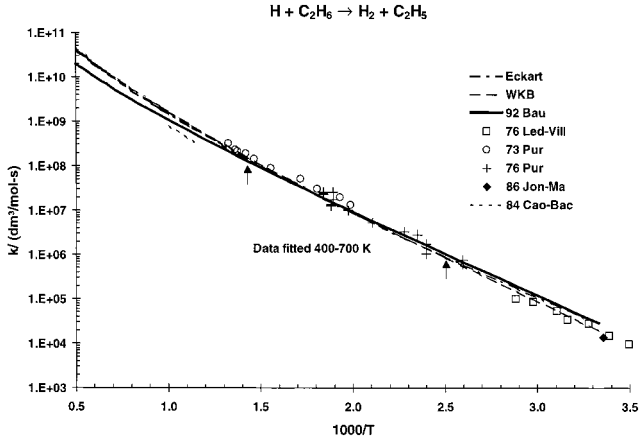

Figure 8. Arrhenius plot of rate constant and TST fits for H + C_2H_6 → C_2H_5 + H_2 reaction. Arrows indicate the temperature range used for fitting TST rates.

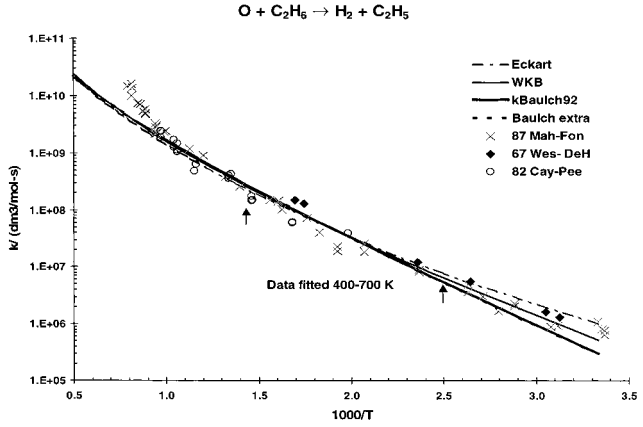

Figure 9. Arrhenius plot of rate constant and TST fits for O + C_2H_6 → C_2H_5 + HO reaction. Arrows indicate the temperature range used for fitting TST rates. "92 Baulch extrapolated" indicates the range were there is no experimental data to support Baulch's 92 recommendation.

approximately the same for all tunneling schemes (9.7 kcal/mol) but somewhat below the QCISD value of 11.0 kcal/mol.

O + C_2H_6 → C_2H_5 + OH. Results from fitting this reaction in the 400−700 K range, shown in Figure 9, differed somewhat below 500 K for the two tunneling corrections employed. The WKB method gave the best results with an rms deviation from Baulch's curve of 19% in the 300−1200 K range, where experimental data were available. The Baulch et al. recommendation is skewed below the reported lower temperature data to take into account Cohen's arguments suggesting that the lower

TABLE 4: Three-Parameter Fits[a]

	WKB tunneling			Eckart tunneling			
reaction	*A*	*B*	*C*	*A*	*B*	*C*	temp range
$H + C_2H_6 \rightarrow H_2 + C_2H_5$	9.888×10^4	1.96	3843.4	4.115×10^3	2.35	3458.1	300−2000
$O + C_2H_6 \rightarrow OH + C_2H_5$	1.494×10^3	2.33	2236.8	16.643	2.88	1651.3	300−2000
$OH + C_2H_6 \rightarrow H_2O + C_2H_5$	1.163×10^4	1.99	661.9	5.743×10^3	2.08	573.8	300−2000
$OH + C_2D_6 \rightarrow HOD + C_2D_5$	4.754×10^3	2.10	962.1	3.626×10^3	2.13	922.9	293−2000
$NH_2 + C_2H_6 \rightarrow NH3 + C_2H_5$	7.800×10^4	1.48	3799.1	57.76	2.36	2755.2	300−1880
$CH_3 + C_2H_6 \rightarrow CH_4 + C_2H_5$	1.239	3.04	5344.7	3.439×10^{-5}	4.33	3808.0	300−2000

[a] $k/(\mathrm{dm^3\ mol^{-1}\ s^{-1}}) = AT^B \exp(-C/T)$.

temperature data was too high.[34] The Eckart correction using the DFT frequency at the transition state overestimates tunneling at low temperatures. However, if the Eckart function is forced to fit the IRC potential, the imaginary frequency decreases from 1363 to 771 cm^{-1} and the resulting curve is very close to that calculated with the WKB scheme. Deviations from Baulch's curve are largest at low temperatures for both kinds of tunneling corrections which predict higher reaction rates. The rates measured by Caymax and Peeters[35] in the 600−1000 K range agree well with both fits; however, data reported by Mahmud et al.[36] at temperatures greater than 1000 K shows distinctly more curvature than expected.

$NH_2 + C_2H_6 \rightarrow C_2H_5 + NH_3$. Experimental data for this reaction are available in the 300−1880 K range[37−39] and as shown in Figure 10, we fit the rates in the range 894−961 K. The Eckart-corrected curve has its largest errors at low temperatures while the deviations of the WKB-corrected data set are distributed over the temperature range, indicating a consistent overestimation of tunneling by the three-parameter Eckart method. The imaginary frequency is lowered by fitting the IRC curve (1275 cm^{-1} compared to 1600 cm^{-1}) and results in smaller tunneling corrections, comparable to the WKB method, with rms deviations of 35.5% and 34.7%, respectively. The resulting activation barriers (9.8 and 10.0 kcal/mol with Eckart and WKB corrections, respectively) are close to 10.2 kcal/mol used be by Lin[5] to fit experimental data, but about 2 kcal/mol lower than those calculated with G2M methods.

$CH_3 + C_2H_6 \rightarrow C_2H_5 + CH_4$. Although experimental data[40,41−43] are only available in the temperature range 1000−1400 K, Baulch[27] et al. have extended their recommendation to the 300−1500 K range based on low-temperature data on isotopic variations. This resulted in an Arrhenius plot with very high curvature (the temperature exponent in their three-parameter expression is 6.0). Our calculations indicate a high degree of tunneling (the WKB correction at 300 K is 38) which accounts for the increased curvature of the Arrhenius plot (Figure 11) and our temperature exponent is 3.0 (see Table 4). The resulting curve obtained with WKB method predicts high-temperature rates between those measured by Roth and Just[42] and Moller et al.[43] The rate constant is too small at low temperatures for there to be any data to compare.

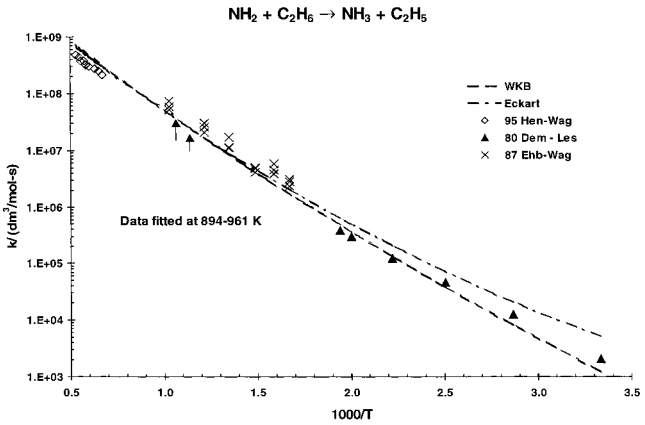

Figure 10. Arrhenius plot of rate constant and TST fits for $NH_2 + C_2H_6 \rightarrow C_2H_5 + NH_3$ reaction. Arrows indicate the temperature range used for fitting TST rates.

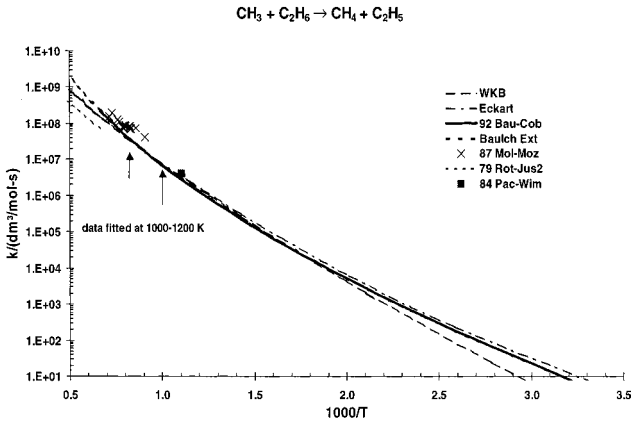

Figure 11. Arrhenius plot of rate constant and TST fits for $CH_3 + C_2H_6 \rightarrow C_2H_5 + CH_4$ reaction. Arrows indicate the temperature range used for fitting TST rates. "92 Baulch extrapolated" indicates the range were there is no experimental data to support Baulch's 92 recommendation.

Conclusions

For all reactions considered except $OH + C_2H_6$, asymmetric Eckart tunneling corrections are larger than WKB at low temperatures and smaller at high temperatures. This is due to the faster decay with temperature of the Eckart transmission probability, in addition to nonclassical reflection effects not accounted for with WKB. We found that the magnitude of the imaginary frequencies calculated with the B3LYP method is often too large compared to that obtained from the curvature of the IRC surface. In the case of $OH + C_2H_6$ the transition state is so early that the IRC curve is poorly represented by an Eckart function and thus tunneling corrections based on Eckart functions are not recommended.

In general, we found that the extrapolations obtained with our method by fitting data in the 400−700 K range are in good agreement with existing experimental data when WKB tunneling corrections are employed. Those obtained from a three-parameter Eckart function have larger deviations but are considerably more efficient to compute because there is no need for detailed knowledge of the IRC surface. Although most of the Eckart tunneling corrections with parameters obtained by fitting an IRC gave results similar to those of the WKB calculations, in some instances the potential differs significantly in shape, thus a good fit is not possible to achieve with a single Eckart function and this method can be unreliable. The differences between these methods are more pronounced at

temperatures below 300 K where tunneling greatly affects the rate constants.

In future work we intend to explore the correlation between the approach in thermochemical kinetics and the results we have obtained. Given the effort involved in the IRC calculation, if a systematic raising of the appropriate transition state frequencies and the neglect of tunneling can reproduce the WKB-corrected quantum/TST method, such an "engineering" approach will facilitate modeling efforts involving large systems of reactions.

Despite the progress in quantum chemical methods, it is not clear that they can accurately and reliably estimate activation barriers. Of the three methods presented here, DFT consistently underestimates the barriers by as much as 6 kcal/mol, whereas MP2 and QCISD(T) overestimate them by as much as 7 kcal/mol. The error of the latter method reduces when progressively larger basis sets are used, at a significant computational cost.

Acknowledgment. D.M.G. was supported by a gift from the Chemical Manufacturer's Association and a grant from NASA's Upper Atmosphere Research Program. J.P.S. and C.B.M. thank LSI Logic Inc. The authors also thank C. González (NIST) and D. Huestis (SRI) for their valuable comments.

References and Notes

(1) Smith, G. P.; Golden, D. M.; Frenklach, M.; Moriarty, N. W.; Eiteneer, B.; Goldenberg, M.; Bowman, C. T.; Hanson, R. K.; Song, S.; Gardiner, W. C. J.; Lissianski, V. V.; Qin, Z. GRI-Mech. http://www.me.berkeley.edu/gri_mech/.

(2) Johnston, H. S. *Gas-Phase Reaction Rate Theory*; Ronald Press Co.: New York, 1966.

(3) Bottoni, A.; Poggi, G. *J. Mol. Struct. Theochem* **1995**, *337*, 161−172.

(4) Jursic, B. S. *J. Mol. Struct. Theochem* **1998**, *428*, 49−54.

(5) Mebel, A. M.; Moskaleva, L. V.; Lin, M. C. *J. Mol. Struct. Theochem* **1999**, *462*, 223−238.

(6) Basch, H.; Hoz, S. *J. Phys. Chem. A* **1997**, *101*, 4416−4431.

(7) Clarke, J. S.; Kroll, J. H.; Donahue, N. M.; Anderson, J. G. *J. Phys. Chem. A* **1998**, *102*, 9847−9857.

(8) Louis, F.; Gonzalez, C. A.; Huie, R. E.; Kurylo, M. J. *J. Phys. Chem. A* **2000**, *104*, 2931−2938.

(9) Schwartz, M.; Marshall, P.; Berry, R. J.; Ehlers, C. J.; Petersson, G. A. *J. Phys. Chem. A* **1998**, *102*, 10074−10081.

(10) Benson, S. W. *Thermochemical Kinetics*; John Wiley & Sons: New York, 1968.

(11) Cohen, N. *Int. J. Chem. Kinet.* **1991**, *23*, 397−417.

(12) Stewart, P. H.; Rothem, T.; Golden, D. M. *22nd Symp. (Int.) Combust., [Proc.]* **1988**.

(13) Rodgers, A. S. *Int. J. Chem. Kinet.* **1993**, *25*, 41−51.

(14) Becke, A. D. *J. Chem. Phys.* **1993**, *98*, 5648−5652.

(15) Baboul, A. G.; Curtiss, L. A.; Redfern, P. C.; Raghavachari, K. *J. Chem. Phys.* **1999**, *110*, 7650−7657.

(16) Bauschlicher, C. W.; Partridge, H. *J. Chem. Phys.* **1995**, *103*, 1788−1791.

(17) Møller, C., Plesset, M. S. *Phys. Rev.* **1934**, 46, 618.

(18) Pople, J. A.; Head-Gordon, M.; Raghavachari, K. *J. Chem. Phys.* **1987**, 87, 5968−5975.

(19) Curtiss, L. A.; Raghavachari, K.; Trucks, G. W.; Pople, J. A. *J. Chem. Phys.* **1991**, *94*, 7221−7230.

(20) Frisch, M. J.; Trucks, G. W.; Schlegel, H. B.; Gill, P. M. W.; Johnson, B. G.; Robb, M. A.; Cheeseman, J. R.; Keith, T.; Petersson, G. A.; Montgomery, J. A.; Raghavachari, K.; Al-Laham, M. A.; Zakrzewski, V. G.; Ortiz, J. V.; Foresman, J. B.; Cioslowski, J.; Stefanov, B. B.; Nanayakkara, A.; Challacombe, M.; Peng, C. Y.; Ayala, P. Y.; Chen, W.; Wong, M. W.; Andres, J. L.; Replogle, E. S.; Gomperts, R.; Martin, R. L.; Fox, D. J.; Binkley, J. S.; Defrees, D. J.; Baker, J.; Stewart, J. P.; Head-Gordon, M.; Gonzalez, C.; Pople, J. A. *Gaussian 94*, Revision E.2; Gaussian, Inc.: Pittsburgh, PA, 1995.

(21) McQuarrie, D. A. *Statistical Thermodynamics*; University Science Books: Mill Valley, CA, 1973.

(22) Pitzer, K. S.; Gwinn, W. D. *J. Chem. Phys.* **1942**, *10*, 428−440.

(23) Eckart, C. *Phys. Rev.* **1930**, *35*, 1303.

(24) Gonzalez, C.; Schlegel, H. B. *J. Chem. Phys.* **1989**, *90*, 2154−2161.

(25) Gonzalez, C.; Schlegel, H. B. *J. Phys. Chem.* **1990**, *94*, 5523−5527.

(26) Sharkey, P.; Smith, I. W. M. *J. Chem. Soc., Faraday Trans.* **1993**, 89, 631−638.

(27) Baulch, D. L. *J. Phys. Chem. Ref. Data* **1992**, 21.

(28) Fenimore, C. P.; Jones, G. W. *9th Symp. (Int.) Combust., [Proc.]* **1963**.

(29) Hu, W. P.; Rossi, I.; Corchado, J. C.; Truhlar, D. G. *J. Phys. Chem. A* **1997**, *101*, 6911−6921.

(30) Tully, F. P.; Droege, A. T.; Koszykowski, M. L.; Melius, C. F. *J. Phys. Chem.* **1986**, *90*, 691−698.

(31) Camilleri, P.; Marshall, R. M.; Purnell, J. H. *J. Chem. Soc., Faraday Trans. 1* **1974**, *70*, 1434−1444.

(32) Jones, D.; Morgan, P. A.; Purnell, J. H. *J. Chem. Soc., Faraday Trans. 1* **1977**, *73*, 1311−1318.

(33) Lede, J.; Villermaux, J. *Can. J. Chem.* **1978**, *56*, 392−401.

(34) Cohen, N. *Int. J. Chem. Kinet.* **1986**, *18*, 59−82.

(35) Caymax, M.; Peeters, J. *19th Symp. (Int.) Combust., [Proc.]* **1982**.

(36) Mahmud, K.; Marshall, P.; Fontijn, A. *J. Chem. Phys.* **1988**, *88*, 2393−2397.

(37) Demissy, M.; Lesclaux, R. *J. Am. Chem. Soc.* **1980**, *102*, 2897−2902.

(38) Hennig, G.; Wagner, H. G. *Ber. Bunsen-Ges. Phys. Chem.* **1995**, *99*, 863−869.

(39) Ehbrecht, J.; Hack, W.; Rouveirolles, P.; Wagner, H. G. *Ber. Bunsen-Ges. Phys. Chem.* **1987**, *91*, 700−708.

(40) Pacey, P. D.; Wimalasena, J. H. *Can. J. Chem.* **1984**, *62*, 293−297.

(41) Lee, W. M.; Yeh, C. T. *J. Phys. Chem.* **1979**, *83*, 771−774.

(42) Roth, P.; Just, T. *Ber. Bunsen-Ges. Phys. Chem.* **1979**, *83*, 577−583.

(43) Moller, W.; Mozzhukhin, E.; Wagner, H. G. *Ber. Bunsen-Ges. Phys. Chem.* **1987**, *91*, 660−666.